

# Bidirectional optical non-reciprocity in a multi-mode cavity optomechanical system

Muhib Ullah,<sup>1</sup> Xihua Yang,<sup>2</sup> and Li-Gang Wang<sup>1,\*</sup>

<sup>1</sup>*Zhejiang Province Key Laboratory of Quantum Technology and Device,*

*Department of Physics, Zhejiang University, Hangzhou 310027, China*

<sup>2</sup>*Department of Physics, Shanghai University, Shanghai 200444, China*

(Dated: September 6, 2021)

Optical non-reciprocity, a phenomenon that allows unidirectional flow of optical field is pivoted on the time reversal symmetry breaking. The symmetry breaking happens in the cavity optomechanical system (COS) due to non uniform radiation pressure as a result of light-matter interaction, and is crucial in building non-reciprocal optical devices. In our proposed COS, we study the non-reciprocal transport of optical signals across two ports via three optical modes optomechanically coupled to the mechanical excitations of two nano-mechanical resonators (NMRs) under the influence of strong classical drive fields and weak probe fields. By tuning different system parameters, we discover the conversion of reciprocal to non-reciprocal signal transmission. We reveal perfect non-reciprocal transmission of output fields when the effective cavity detuning parameters are near resonant to the NMRs' frequencies. The unidirectional non-reciprocal signal transport is robust to the optomechanical coupling parameters at resonance conditions. Moreover, the cavities' photon loss rates play an inevitable role in the unidirectional flow of signal across the two ports. Bidirectional transmission can be fully controlled by the phase changes associated with the incoming probe and drive fields via two ports. Our scheme may provide a foundation for the compact non-reciprocal communication and quantum information processing, thus enabling new devices that route photons in unconventional ways such as all-optical diodes, optical transistors and optical switches.

## I. INTRODUCTION

Non-reciprocity is a phenomenon in certain devices that allows signal to pass through in one direction, but block it in the opposite, and requisite in a broad range of applications such as invisibility or cloaking, and noise free information processing [1]. Optical non-reciprocity has originated from breaking the Lorentz reciprocity theorem [2]. Apart from that, optical non-reciprocity has been realized in magneto-optical Faraday effect [3–9], but the major flaw in these devices is their inconvenience in integration because of some issues such as crosstalk caused by the magnetic field, ill-suitableness for sensitive superconducting circuits as their strong magnetic fields are highly disruptive and need strong shielding, and lattice mismatches between magneto-optic materials and silicon [10]. In addition, magneto-optical materials manifest remarkable loss at optical frequencies, that is, the order of  $100 \text{ dB cm}^{-1}$ , making them sub-optimal solutions for high-efficiency devices. As an alternate to magnet based non-reciprocal devices, a number of techniques have been practiced using a microwave chip-level system. One approach used is establishing an artificial magnetic field by modulating the parametric coupling between the modes of a network thus making the system non-reciprocal at the ports [11–13]. The second technique is the phase matching of a parametric interaction that leads to non-reciprocal behavior of the communicating signal, since the signal only interacts with the pump when co-propagating with it and not in the opposite di-

rection. This causes traveling-wave amplification to be directional [13–16].

The approach for on-chip optical non-reciprocity has also been used recently by using a strong optomechanical interaction between the external fields and microring resonators [17], and has been experimentally demonstrated using a silica microsphere resonator, recently [18]. In a similar fashion, an optomechanical circulator and directional amplifier in a two-tapered fiber-coupled silica micro-resonator have been proposed to perform as an add-drop filter, and they may be switched to circulator mode or directional amplifier mode via a simple change in the control field [19]. It has been accredited that the non-reciprocal signal transfer between two optical modes mediated by mechanical mode can be realized with suitable optical driving [20, 21]. Additionally, these modes in cavity optomechanics can also result in some other interesting effects like ground-state cooling of an NMR [22], steady-state light-mechanical quantum steerable correlations in a cavity optomechanical system (COS) [23], slow-to-fast light tuning and single-to-double optomechanically induced transparency (analogous to electromagnetically induced transparency) [24], flexible manipulation on Goos-Hänchen shift as a classical application of COS [25], Fano resonances [26], superradiance [27], and optomechanically induced opacity and amplification in a quadratically coupled COS [28]. Apart from that, Peterson *et al.* have further demonstrated an efficient frequency-converting microwave isolator, stemmed on the optomechanical interactions between electromagnetic fields and a mechanically compliant vacuum-gap capacitor, which does not require a static magnetic field and allows a dynamic control of the direction of isolation [29]. Bernier *et al.* have experimentally realized

\*Electronic address: sxwlg@yahoo.com

the non-reciprocal scheme in an optomechanical system using a superconducting circuit in which mechanical motion is capacitively coupled to a multimode microwave circuit [30]. Similarly, Barzanjeh *et al.* have presented an on-chip microwave circulator using a frequency tunable silicon-on-insulator electromechanical system to investigate non-reciprocity via two output ports and is also compatible with superconducting qubits [31].

Fetching an insight from the above discussion, we introduce a scheme to achieve the bidirectional non-reciprocal signal transmission using purely optomechanical interaction in the presence of a partial beam splitter (BS). The setup consists of two ports (left and right) through which the signal exchange occurs. The external fields interact with the cavity modes and thus with the nano-mechanical resonators' (NMRs) phonons via radiation pressure force, which induces effective nonlinearity into the system and breaks the time reversal symmetry. These factors ultimately are accountable for the optical non-reciprocal behavior of the system to incoming light fields. Non-reciprocal process as a result of interference due to different phases has been discussed in a two-mode cavity system with two mechanical modes [32, 33]. Very recently, in a letter, a configurable and directional electromagnetic signal transmission has been shown to be obtained in an optomechanical system by designing a loop of interactions in the synthetic plane generated by driven Floquet modes on one hand and multiple mechanical modes on the other hand, to realize a microwave isolator and a directional amplifier [34].

This article is organized as follows. In section II, we present the model of the multi-mode COS and calculate the analytical results for the output fields of both ports 1 and 2. In section III, we analyze and discuss our results numerically and explain the behavior of output signal transport under different system parameters. In the last section, we conclude our work.

## II. MODEL AND CALCULATIONS

The proposed model shown in Fig. 1 is a two-port COS that is composed of two partially transparent mirrors ( $M_1$  and  $M_2$ ) fixed opposite to each other and two perfectly reflecting movable NMRs oscillating along the same axis and a partial beam splitter is placed between them. The NMRs oscillate around their equilibrium positions with small displacements  $q_1$  and  $q_2$ , usually in the order of  $10^{-9}$  m. The fixed mirrors  $M_1$  and  $M_2$  are separated in such a way that a standing wave is formed in between as represented by a straight horizontal arrow. This mirror setup form three cavity modes represented by  $a_1$ ,  $a_2$  and  $a_3$  interconnected by means of NMRs' mechanical excitations. Two external classical fields, i.e., strong drive fields (field strengths  $\Omega_{d1}$ ,  $\Omega_{d2}$  and frequency  $\omega_d$ ) and a weak probe field (field strengths  $\Omega_{p1}$ ,  $\Omega_{p2}$  and frequency  $\omega_p$ ) are injected from both ports (left and right) to the COS setup. After interacting with the cavity dynamics,

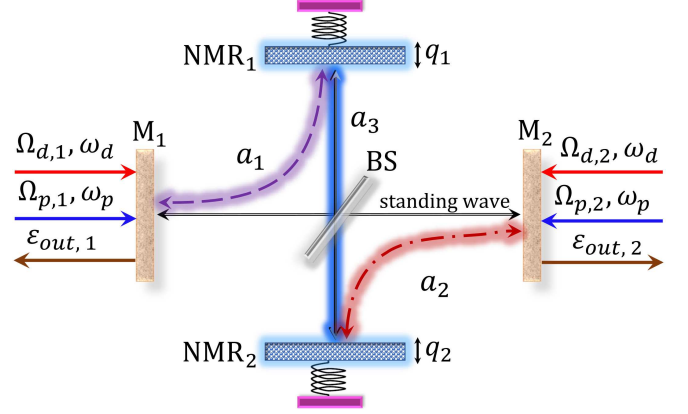


FIG. 1: Schematic of a two ports multi-mode optomechanical cavity setup excited by external classical fields. The setup comprises two fixed partially transparent mirrors ( $M_1$  and  $M_2$ ) and two movable perfectly reflecting nano-mechanical resonators ( $NMR_1$  and  $NMR_2$ ) with small displacements  $q_1$  and  $q_2$  from their respective equilibrium positions. A partial BS is placed at the center inside the mirrors configuration. There are three optical (photonic) modes  $a_1$ ,  $a_2$  and  $a_3$ , and two mechanical (phononic) modes ( $b_1$  and  $b_2$ ) in this system interconnected via optomechanical couplings, while a standing wave between  $M_1$  and  $M_2$  represented by a straight horizontal arrow is formed. Two classical fields, that is, strong drive field with strengths  $\Omega_{d1}$  and  $\Omega_{d2}$  (frequency  $\omega_d$ ), and weak probe field having strengths  $\Omega_{p1}$  and  $\Omega_{p2}$  (frequency  $\omega_p$ ) interact with the cavity system from the respective sides via  $M_1$  and  $M_2$ , whereas the output fields ( $\varepsilon_{out,1}$  and  $\varepsilon_{out,2}$ ) can be drawn out via left and right port, respectively.

the output probe fields ( $\varepsilon_{out,1}$ ,  $\varepsilon_{out,2}$ ) can be collected at the left and right ports, respectively.

The Hamiltonian for COS in the frame rotating at the drive field frequency  $\omega_d$  can be given as

$$H_T = \sum_{i=1}^3 \Delta_{ai} a_i^\dagger a_i + \sum_{j=1}^2 \omega_{mj} b_j^\dagger b_j + \sum_{i=1}^2 O_{mi} a_i^\dagger a_i (b_i^\dagger + b_i) + O_{m31} a_3^\dagger a_3 (b_1^\dagger + b_1) + O_{m32} a_3^\dagger a_3 (b_2^\dagger + b_2) + \sum_{j=1}^2 \sum_{k=1}^3 i \Omega_{dj} (e^{i\Phi_{dj}} a_k^\dagger - e^{-i\Phi_{dj}} a_k) + \sum_{j=1}^2 \sum_{k=1}^3 i \Omega_{pj} (e^{-i(\Delta_p t - \Phi_{pj})} a_k^\dagger - H.c.), \quad (1)$$

where  $\Delta_{a1} = \omega_{a1} - \omega_d$ ,  $\Delta_{a2} = \omega_{a2} - \omega_d$  and  $\Delta_{a3} = \omega_{a3} - \omega_d$  are the cavity-drive field detunings, whereas  $\Delta_p = \omega_p - \omega_d$  denote the probe-drive field detuning. In Eq. (1), the first term in the Hamiltonian represents the energy of cavity mode  $a_i$  with  $i = 1, 2, 3$  the number of cavities. The second term in the expression shows the energy of  $j$ th bosonic mode  $b_j$  with  $j = 1, 2$ . The third term accounts for the optomechanical interaction between cavity modes and mechanical modes that come into existence because of radiation pressure, while the

parameters  $O_{mi}$  ( $i = 1, 2$ ) are the optomechanical coupling strengths between the cavity photons and NMRs. The fourth and fifth terms are associated with the optomechanical interaction between the cavity mode  $a_3$  and two NMRs having  $O_{m31}$  and  $O_{m32}$  as the optomechanical couplings between them. These terms are crucial for the realization of optical non-reciprocity in our proposed cavity setup. Non-reciprocity is lost when these couplings vanish or equal to zero. The last two terms correspond to the interaction of strong classical drive fields and weak probe fields with the cavity modes, respectively, with H.c. as the Hermitian conjugate terms.

Considering that the system may be dissipative, we use the Heisenberg's equations of motion (so-called quantum langevin equation) along with damping terms given as [35, 36]

$$\dot{Z} = -\frac{i}{\hbar}[Z, H_T] - \gamma Z + N, \quad (2)$$

where  $Z \in (a_1, a_2, a_3, b_1, b_2)$  is a general operator variable,  $\gamma$  is the corresponding damping term, and the term  $N$  is the quantum white noise (Brownian noise) whose value averages to zero. Without loss of generality, the reduced Planck's constant ( $\hbar$ ) is considered as equal to 1. We use Eq. (2) to obtain the equation of motion for every operator variable and explore the dynamics of the system. Furthermore, the differential equations obtained by substituting Eq. (1) into Eq. (2) are the coupled nonlinear equations that need to be decoupled. By the application of factorization theorem, that is,  $\langle ab \rangle = \langle a \rangle \langle b \rangle$  those differential equations can be decoupled [35, 37]. Through the above process, we obtain the following mean-value equations

$$\begin{aligned} \langle \dot{a}_1 \rangle = & -(\kappa_1 + i\Delta_{a1})\langle a_1 \rangle + iO_{m1}(\langle b_1^\dagger \rangle + \langle b_1 \rangle)\langle a_1 \rangle \\ & + \sum_{j=1}^2 \Omega_{dj} e^{i\Phi_{dj}} + \sum_{k=1}^2 \Omega_{pj} e^{-i(\Delta_p t - \Phi_{pk})}, \end{aligned} \quad (3a)$$

$$\begin{aligned} \langle \dot{a}_2 \rangle = & -(\kappa_2 + i\Delta_{a2})\langle a_2 \rangle + iO_{m2}(\langle b_2^\dagger \rangle + \langle b_2 \rangle)\langle a_2 \rangle \\ & + \sum_{j=1}^2 \Omega_{dj} e^{i\Phi_{dj}} + \sum_{k=1}^2 \Omega_{pj} e^{-i(\Delta_p t - \Phi_{pk})}, \end{aligned} \quad (3b)$$

$$\begin{aligned} \langle \dot{a}_3 \rangle = & -(\kappa_3 + i\Delta_{a3})\langle a_3 \rangle + iO_{m31}(\langle b_1^\dagger \rangle + \langle b_1 \rangle)\langle a_3 \rangle \\ & + iO_{m32}(\langle b_2^\dagger \rangle + \langle b_2 \rangle)\langle a_3 \rangle + \sum_{j=1}^2 \Omega_{dj} e^{i\Phi_{dj}} \\ & + \sum_{k=1}^2 \Omega_{pj} e^{-i(\Delta_p t - \Phi_{pk})}, \end{aligned} \quad (3c)$$

$$\langle \dot{b}_1 \rangle = -(\gamma_1 + i\omega_{m1})\langle b_1 \rangle + iO_{m31}\langle a_3^\dagger \rangle \langle a_3 \rangle, \quad (3d)$$

$$\langle \dot{b}_2 \rangle = -(\gamma_2 + i\omega_{m2})\langle b_2 \rangle + iO_{m32}\langle a_3^\dagger \rangle \langle a_3 \rangle. \quad (3e)$$

It is difficult to solve the master equation exactly because of the existence of the nonlinear terms. Hence we apply the linearization approach by assuming that each operator in the system can be written as the sum of its mean

value and a small fluctuation, i.e., applying an ansatz of the form given by  $\langle Z \rangle = Z_s + \delta Z$ , ( $Z \in a_1, a_2, a_3, b_1, b_2$ ), where  $Z_s$  stands for the steady-state value and  $\delta Z$  for the small fluctuations around the steady-state values of all the operator variables under observation. The fluctuations for each variable can be addressed as

$$\begin{aligned} \delta a_1 & \rightarrow \delta \tilde{a}_1 e^{-i\Delta_1 t}, \quad \delta a_2 \rightarrow \delta \tilde{a}_2 e^{-i\Delta_2 t}, \\ \delta a_3 & \rightarrow \delta \tilde{a}_3 e^{-i\Delta_3 t}, \quad \delta b_1 \rightarrow \delta \tilde{b}_1 e^{-i\omega_{m1} t}, \\ \delta b_2 & \rightarrow \delta \tilde{b}_2 e^{-i\omega_{m2} t}, \end{aligned} \quad (4)$$

where  $\Delta_i$  ( $i = 1, 2, 3$ ) is the effective cavity detuning and  $\omega_{mj}$  ( $j = 1, 2$ ) is the NMR's resonance frequency. As the drive fields are much stronger than the probe fields, we can use the conditions  $|a_{is}| \gg \delta a_i$  ( $i = 1, 2, 3$ ) and  $|b_{js}| \gg \delta b_j$  ( $j = 1, 2$ ) in the absence of the probe fields  $\Omega_{p1}$  and  $\Omega_{p2}$ , and finally get the steady-state solutions according to the method in Ref. [38]

$$a_{1s} = \frac{\Omega_{d1} e^{i\Phi_{d1}} + \Omega_{d2} e^{i\Phi_{d2}}}{(\kappa_1 + i\Delta_1)}, \quad b_{1s} = \frac{iO_{m31} |a_{3s}|^2}{(\gamma_1 + i\omega_{m1})}, \quad (5a)$$

$$a_{2s} = \frac{\Omega_{d1} e^{i\Phi_{d1}} + \Omega_{d2} e^{i\Phi_{d2}}}{(\kappa_2 + i\Delta_2)}, \quad b_{2s} = \frac{iO_{m32} |a_{3s}|^2}{(\gamma_2 + i\omega_{m2})}, \quad (5b)$$

$$a_{3s} = \frac{\Omega_{d1} e^{i\Phi_{d1}} + \Omega_{d2} e^{i\Phi_{d2}}}{(\kappa_3 + i\Delta_3)}, \quad (5c)$$

were  $\Delta_1 = \Delta_{a1} - O_{m1}(b_{1s} + b_{1s}^*)$ ,  $\Delta_2 = \Delta_{a2} - O_{m2}(b_{2s} + b_{2s}^*)$  and  $\Delta_3 = \Delta_{a3} - O_{m31}(b_{1s} + b_{1s}^*) - O_{m32}(b_{2s} + b_{2s}^*)$  are the effective cavity detunings of the cavity modes  $a_1$ ,  $a_2$  and  $a_3$ , respectively. In Eq. 5(a-c), the expressions  $a_{is}$  ( $i = 1, 2, 3$ ) and  $b_{js}$  ( $j = 1, 2$ ) are the steady-state solutions of optical modes and mechanical modes, respectively. To find out the role of the weak probe fields in the system dynamics, the small fluctuations are taken into consideration by using the assumption given in Eq. (4), and only slowly moving linear terms are entertained, whereas fast oscillating terms are ignored. Thus the linearized equations of motion for the fluctuation part of the variable operators can be derived as

$$\begin{aligned} \delta \dot{a}_1 = & -(\kappa_1 + i\Delta_{a1})\delta \tilde{a}_1 + iO_{m1}a_{1s}\delta \tilde{b}_1 \\ & + \Omega_{p1} e^{i\Phi_{p1}} e^{-ix_1 t} + \Omega_{p2} e^{i\Phi_{p2}} e^{-ix_1 t}, \end{aligned} \quad (6)$$

where  $x_1 = \omega_p - \omega_d - \omega_{m1} = \Delta_p - \omega_{m1}$  is the probe detuning and the movable mirror resonance frequency's difference. Expressions for  $\delta \dot{a}_2$  and  $\delta \dot{a}_3$  can be solved alike as  $\delta \dot{a}_1$ , and they are given as

$$\begin{aligned} \delta \dot{a}_2 = & -(\kappa_2 + i\Delta_{a2})\delta \tilde{a}_2 + iO_{m2}a_{2s}\delta \tilde{b}_2 + \Omega_{p1} e^{i\Phi_{p1}} e^{-ix_2 t} \\ & + \Omega_{p2} e^{i\Phi_{p2}} e^{-ix_2 t}, \end{aligned} \quad (7)$$

$$\begin{aligned} \delta \dot{a}_3 = & -(\kappa_3 + i\Delta_{a3})\delta \tilde{a}_3 + iO_{m31}a_{3s}\delta \tilde{b}_1 + iO_{m32}a_{3s}\delta \tilde{b}_2 \\ & + \Omega_{p1} e^{i\Phi_{p1}} e^{-ix_3 t} + \Omega_{p2} e^{i\Phi_{p2}} e^{-ix_3 t}, \end{aligned} \quad (8)$$

where the parameters  $x_2 = \Delta_p - \omega_{m2}$  and  $x_3 = \Delta_p - \Delta_3$ . Without loss of generality, all the cavity modes are supposed to be driven in the mechanical red sidebands

with  $\Delta_1 = \Delta_2 = \Delta_3 = \omega_{m1} = \omega_{m2} = \omega_m$ . Therefore,  $x_1 = x_2 = x_3 = x$  and the system is operated in the resolved sideband regime with the condition that  $\omega_m \gg \kappa_j$ , where  $j = 1, 2, 3$ . With the above assumptions, the coefficients of the mechanical mode fluctuation operators  $\delta\tilde{b}_1$  and  $\delta\tilde{b}_2$  can be simplified as

$$\dot{\delta\tilde{b}}_1 = -(\gamma_1 + i\omega_{m1})\delta\tilde{b}_1 + iO_{m31}a_{3s}^*\delta\tilde{a}_3, \quad (9)$$

$$\dot{\delta\tilde{b}}_2 = -(\gamma_2 + i\omega_{m2})\delta\tilde{b}_2 + iO_{m32}a_{3s}^*\delta\tilde{a}_3. \quad (10)$$

The fluctuation values of the operator variables can be further expanded to obtain the solution easily by using the ansatz given below.

$$\delta\tilde{y} = \delta\tilde{y}_+e^{-ixt} + \delta\tilde{y}_-e^{ixt}, \quad (11)$$

where  $\delta\tilde{y} = \delta\tilde{a}_1, \delta\tilde{a}_2, \delta\tilde{a}_3, \delta\tilde{b}_1$ , and  $\delta\tilde{b}_2$  are the fluctuation variables under study. By substituting Eq. (11) into Eqs. (6)-(10), we achieve the simplified fluctuation operator coefficients for the optical cavity modes as

$$\delta\tilde{a}_{1+} = \frac{iO_{m1}a_{1s}\delta\tilde{b}_{1+} + \sum_{j=1}^2 \Omega_{pj}e^{i\Phi_{pj}}}{(\kappa_1 + i\Delta_{a1} - ix)}, \quad (12)$$

$$\delta\tilde{a}_{2+} = \frac{iO_{m2}a_{2s}\delta\tilde{b}_{2+} + \sum_{j=1}^2 \Omega_{pj}e^{i\Phi_{pj}}}{(\kappa_2 + i\Delta_{a2} - ix)}, \quad (13)$$

$$\delta\tilde{a}_{3+} = \frac{iO_{m31}a_{3s}\delta\tilde{b}_{1+} + iO_{m32}a_{3s}\delta\tilde{b}_{2+} + \sum_{j=1}^2 \Omega_{pj}e^{i\Phi_{pj}}}{(\kappa_3 + i\Delta_{a3} - ix)}, \quad (14)$$

whereas the expressions for the coefficients associated with the mechanical mode fluctuation operators can be calculated and simplified in similar fashion by substitution of Eq. (11) into Eqs. (6)-(10) and can be written as

$$\delta\tilde{b}_{1+} = \frac{iO_{m31}a_{3s}^*\delta\tilde{a}_{3+}}{(\gamma_1 + i\omega_{m1} - ix)}, \quad (15)$$

$$\delta\tilde{b}_{2+} = \frac{iO_{m32}a_{3s}^*\delta\tilde{a}_{3+}}{(\gamma_2 + i\omega_{m2} - ix)}. \quad (16)$$

As the transmission happens via fixed mirrors (left  $M_1$  and right  $M_2$ ) that are connected to the cavity modes  $a_1$  and  $a_2$ , respectively, we calculate the corresponding coefficients  $\delta\tilde{a}_{1+}$  and  $\delta\tilde{a}_{2+}$ . Therefore, we apply a lengthy and tiresome but straight forward substitution method to Eqs. (12)-(16) and obtain the required analytical expressions for  $\delta\tilde{a}_{1+}$  and  $\delta\tilde{a}_{2+}$  as

$$\delta\tilde{a}_{1+} = -\frac{D[V_2(U_3V_1 - O_{m1}O_{m31}a_{1s}a_{3s}^*) + |a_{3s}|^2(O_{m31}^2V_2 + O_{m32}^2V_1)]}{U_1[U_3V_1V_2 + |a_{3s}|^2(O_{m31}^2V_2 + O_{m32}^2V_1)]}, \quad (17)$$

$$\delta\tilde{a}_{2+} = -\frac{D[V_1(U_3V_2 + O_{m2}O_{m32}a_{2s}a_{3s}^*) + |a_{3s}|^2(O_{m31}^2V_2 + O_{m32}^2V_1)]}{U_2[U_3V_1V_2 + |a_{3s}|^2(O_{m31}^2V_2 + O_{m32}^2V_1)]}, \quad (18)$$

where  $D = \Omega_{p1}e^{i\Phi_{p1}} + \Omega_{p2}e^{i\Phi_{p2}}$ , while  $U_1 = ix - i\Delta_{a1} - \kappa_1$ ,  $U_2 = ix - i\Delta_{a2} - \kappa_2$ ,  $U_3 = ix - i\Delta_{a3} - \kappa_3$ ,  $V_1 = ix - i\omega_{m1} - \gamma_1$  and  $V_2 = ix - i\omega_{m2} - \gamma_2$  are the parametric symbols used in Eqs. (17) and (18).

To obtain output fields ( $E_{\text{out},1}$  and  $E_{\text{out},2}$ ) and study its non-reciprocal behavior through both the output ports in such an optomechanical system, input-output relation is convenient to be used as follows [38–40].

$$E_{\text{out}}(t) + E_{\text{in}}(t) = 2\kappa\langle a \rangle, \quad (19)$$

where  $E_{\text{out}}(t) = E_{\text{out}+}e^{-ixt} + E_{\text{out}-}e^{ixt}$  is the output field, generally speaking, and  $E_{\text{in}} = \Omega_{pj}e^{-ixt}$  ( $j = 1, 2$ ) is the input probe light field signal expression entering the system from both ports, while  $2\kappa\langle a \rangle$  is used for the

output field coefficient. By putting the values of above parameters in Eq. (19), we obtain the explicit input-output relation for the system under study as

$$E_{\text{out}j+}e^{-ixt} + E_{\text{out}j-}e^{ixt} + \Omega_{pj}e^{-ixt} = 2\kappa_j\langle a_j \rangle, \quad (20)$$

where ( $j = 1, 2$ ) and  $\langle a_j \rangle = \delta\tilde{a}_{j+}e^{-ixt} + \delta\tilde{a}_{j-}e^{ixt}$ . By replacing the value of  $\langle a_j \rangle$  in Eq. (20), we obtain the output field expressions for both routes, i.e., ports 1 and 2,

$$\begin{aligned} &E_{\text{out}1+}e^{-ixt} + E_{\text{out}1-}e^{ixt} + \Omega_{p1}e^{-ixt} \\ &= 2\kappa_1\delta\tilde{a}_{j+}e^{-ixt} + \delta\tilde{a}_{j-}e^{ixt}. \end{aligned} \quad (21)$$

Equating both sides of Eq. (21) with respect to  $e^{-ixt}$  we

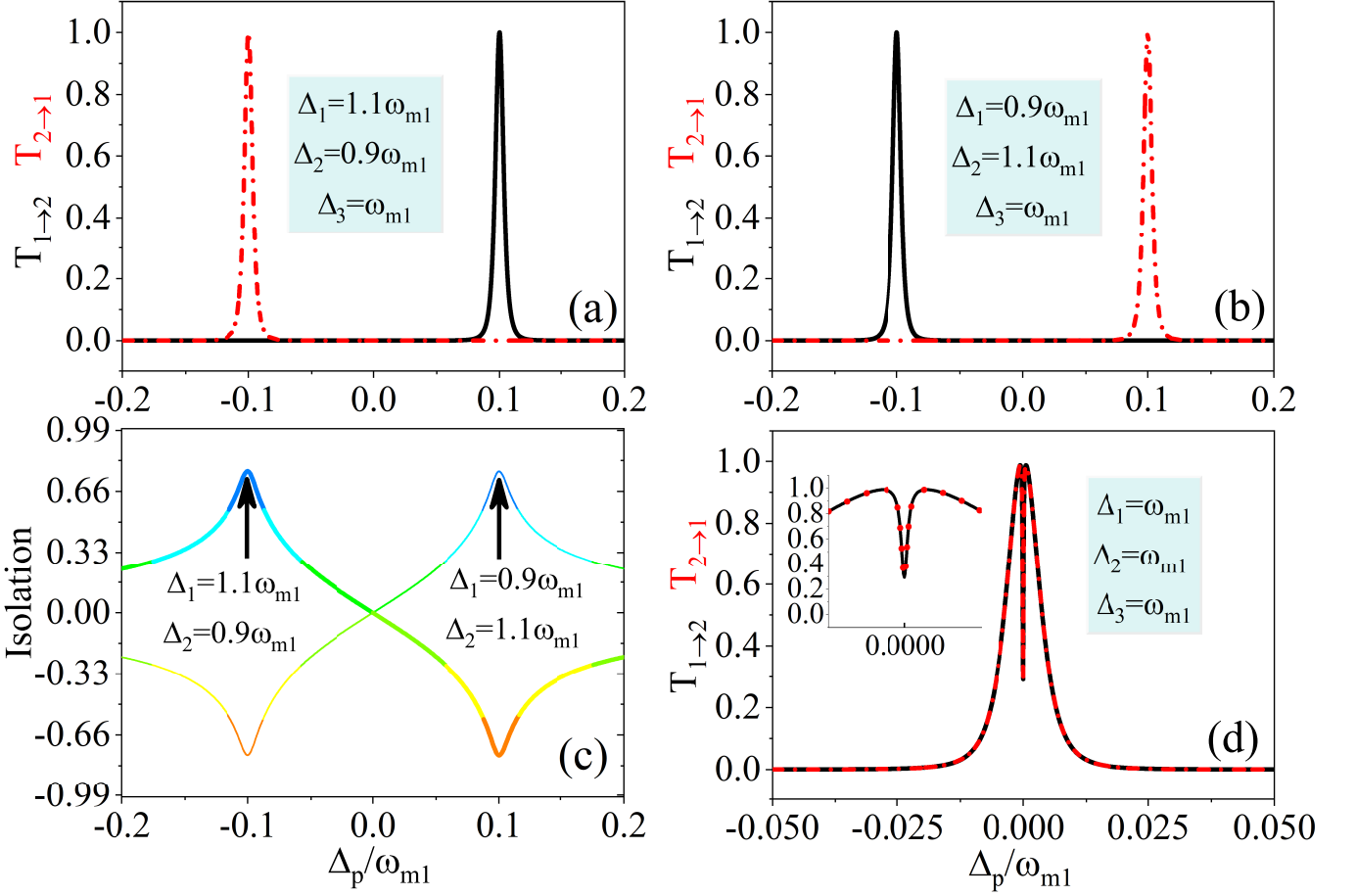


FIG. 2: Transmission intensities  $T_{2 \rightarrow 1}$  and  $T_{1 \rightarrow 2}$  as a function of the probe-drive field detuning  $\Delta_p$  under different values of the effective cavity detunings: (a)  $\Delta_1 = 1.1\omega_{m1}$ ,  $\Delta_2 = 0.9\omega_{m1}$ , (b)  $\Delta_1 = 0.9\omega_{m1}$ ,  $\Delta_2 = 1.1\omega_{m1}$ , (c) The isolation ratio between the transmissions across two ports for varying values of  $\Delta_i$  ( $i = 1, 2$ ), and (d) the same values  $\Delta_1 = \omega_{m1}$ ,  $\Delta_2 = \omega_{m1}$ . The general parameters are given as  $\omega_{m1}/2\pi = \omega_{m2}/2\pi = 12.6$  GHz,  $\kappa_1/2\pi = \kappa_2/2\pi = \kappa_3/2\pi = 73$  MHz,  $\gamma_1/2\pi = \gamma_2/2\pi = 88$  kHz,  $O_{m1}/2\pi = O_{m2}/2\pi = O_{m31}/2\pi = O_{m32}/2\pi = 1.5$  MHz,  $L_i = L_{3i} = 5.19$  mm ( $i = 1, 2$ ),  $m_{\text{eff},j} = 20$   $\mu\text{g}$  ( $j = 1, 2$ ),  $\Phi_{d1} = \Phi_{d2} = \Phi_{p1} = \Phi_{p2} = 0$ ,  $\Omega_{d1} = \Omega_{d2} = 2\omega_{m1}$ , and  $\Omega_{p1} = \Omega_{p2} = 0.2\omega_{m1}$ .

obtain the output field expression at port 1 as

$$E_{\text{out}1+} = \varepsilon_{\text{out},1} = 2\kappa_1\delta\tilde{a}_{1+} - \Omega_{p1}. \quad (22)$$

Similarly, for port 2 the output field relation can be derived as

$$E_{\text{out}2+} = \varepsilon_{\text{out},2} = 2\kappa_2\delta\tilde{a}_{2+} - \Omega_{p2}. \quad (23)$$

The expressions of the transmission amplitudes of both ports are given as [41]

$$T_{2 \rightarrow 1} = |\varepsilon_{\text{out},1}/\Omega_{p2}|^2 = \left| \frac{2\kappa_1\delta\tilde{a}_{1+} - \Omega_{p1}}{\Omega_{p2}} \right|^2, \quad (24)$$

$$T_{1 \rightarrow 2} = |\varepsilon_{\text{out},2}/\Omega_{p1}|^2 = \left| \frac{2\kappa_2\delta\tilde{a}_{2+} - \Omega_{p2}}{\Omega_{p1}} \right|^2, \quad (25)$$

where the strengths of probe light field injected to the system from either port are considered same, quantitatively.

### III. RESULTS AND DISCUSSION

In this section, we will numerically investigate the non-reciprocal behavior of the output signals using the COS scheme with two signal exchange ports. The vital role responsible for this phenomenon is played by the optomechanical interactions between the cavity photons with their respective NMRs' phonons in the presence of partially transmitting BS. For numerical simulations, we consider the practically realizable parameters from a recent experimental work whose values are given as [42]  $\omega_{m1}/2\pi = \omega_{m2}/2\pi = 12.6$  GHz,  $\kappa_1/2\pi = \kappa_2/2\pi = \kappa_3/2\pi = 73$  MHz,  $\gamma_1/2\pi = \gamma_2/2\pi = 88$  kHz,  $O_{m1}/2\pi = O_{m2}/2\pi = O_{m31}/2\pi = O_{m32}/2\pi = 1.5$  MHz,  $L_i = L_{3i} = 5.19$  mm ( $i = 1, 2$ ),  $m_{\text{eff},j} = 20$   $\mu\text{g}$  ( $j = 1, 2$ ),  $\Phi_{d1} = \Phi_{d2} = \Phi_{p1} = \Phi_{p2} = 0$ ,  $\Omega_{d1} = \Omega_{d2} = 2\omega_{m1}$ , and  $\Omega_{p1} = \Omega_{p2} = 0.2\omega_{m1}$ . Our proposed COS can offer an excellent control and manipulation ability to the non-reciprocal transmission. This proposal could be very crit-

ical in the quantum information processing, optical sensors, optical switches, isolators, full-duplex signal transmission and upcoming quantum nanotechnologies.

### A. Tuning $\Delta_1$ and $\Delta_2$ to control non-reciprocity

The non-reciprocal phenomenon discussed here is based on the interference effect at near resonance conditions. The effective cavity detunings  $\Delta_i$  ( $i = 1, 2$ ) play a basic role in controlling the signal transmission. A slight change in the values of  $\Delta_i$  from the resonance value brings in a perfect non-reciprocal transmission around the origin as shown in Fig. 2. By choosing the values  $\Delta_1 = 1.1\omega_{m1}$  and  $\Delta_2 = 0.9\omega_{m1}$ , a perfect blockade of the probe signal  $T_{1 \rightarrow 2}$  and transmission  $T_{2 \rightarrow 1}$  at  $\Delta_p = -0.1\omega_{m1}$  (where the peak lies) on the frequency axis is achieved as depicted in Fig. 2(a). Likewise, at  $\Delta_p = 0.1\omega_{m1}$  on the positive frequency axis, the scenario changes and the signal transfer  $T_{1 \rightarrow 2}$  is permitted while  $T_{2 \rightarrow 1}$  is completely blocked. To fully uncover the contribution of  $\Delta_i$  to the non-reciprocity phenomenon, the values are chosen to be  $\Delta_1 = 0.9\omega_{m1}$  and  $\Delta_2 = 1.1\omega_{m1}$ , so the transmission curve positions for both  $T_{1 \rightarrow 2}$  and  $T_{2 \rightarrow 1}$  on the frequency axis are switched oppositely to the previous case [see Fig. 2(a)] as shown in Fig. 2(b). In both sub figures mentioned above, the probe-field transfer via either port occurs because of constructive interference between the probe field-induced cavity field and the NMRs' excitations (resonance frequencies), while the transmission blockade comes into play due to the destructive interference happening at the near-resonant conditions, and thus no probe signal is received at the output port. There is no signal transfer seen at either port for the frequencies other than mentioned above. Moreover, these interference patterns depend on the cavity detunings, since the radiation pressure vary with the change in  $\Delta_i$  value which ultimately is accountable for breaking the time reversal symmetry and we obtain the non-reciprocal transmission. Hence, by tuning the  $\Delta_i$  value, the non-reciprocal output signal tranger via output ports can observed at a certain frequency range by using our proposed setup. Figure 2(c) shows the isolation, which is the ratio of  $T_{2 \rightarrow 1}$  to  $T_{1 \rightarrow 2}$  transmissions of output signals and is defined by the relation  $\text{Isolation} = \text{Log10} \left[ \left| \frac{T_{2 \rightarrow 1}}{T_{1 \rightarrow 2}} \right| \right]$ . Its curves reveal the quality or effeciency of non-reciprocal transmission, where its maxima and minima signify the perfectness of non-reciprocal behavior at those specific points. The positive and negative magnitudes of the curves show the non-reciprocal transmission happening along positive and negative frequency axis, respectively, around the origin. The Isolation curve remains zero for the reciprocal transmission (not shown in Fig. 2(c)). Unlike the above-mentioned two cases where both the effective cavity detunings are near-resonant with the NMRs' excitations [see Figs. 2(a) and 2(b)], a total reciprocal output field transmission can be noted when  $\Delta_i = \omega_{m1}$ ,

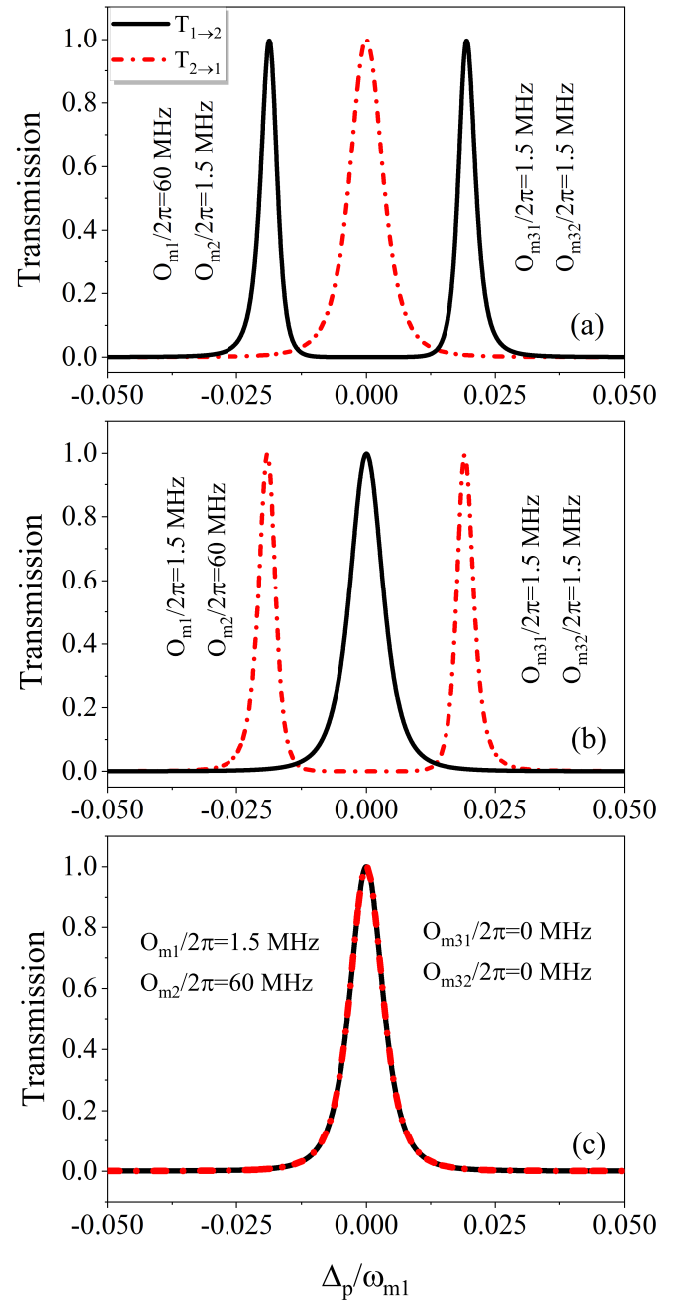


FIG. 3: Transmission intensities  $T_{2 \rightarrow 1}$  and  $T_{1 \rightarrow 2}$  as a function of the probe-drive field detuning  $\Delta_p$  under different values of optomechanical coupling strengths  $O_{m1}$ ,  $O_{m2}$ ,  $O_{m31}$  and  $O_{m32}$ : (a)  $O_{m1}/2\pi = 60$  MHz,  $O_{m2}/2\pi = O_{m31}/2\pi = O_{m32}/2\pi = 1.5$  MHz, (b)  $O_{m1}/2\pi = 1.5$  MHz,  $O_{m2}/2\pi = 60$  MHz,  $O_{m31}/2\pi = O_{m32}/2\pi = 1.5$  MHz, and (c)  $O_{m1}/2\pi = 1.5$  MHz,  $O_{m2}/2\pi = 60$  MHz,  $O_{m31}/2\pi = O_{m32}/2\pi = 0$  MHz. The general parameters are given as  $\Delta_1 = \Delta_2 = \Delta_3 = \omega_{m1}$ . Other values are same as mentioned in Fig. 2.

that is, the effective cavity detunings are at exact resonance with mechanical resonator's frequency at the origin as shown in Fig. 2(d). The small inset within Fig. 2(c) shows a dip in both ports' transmission curves.

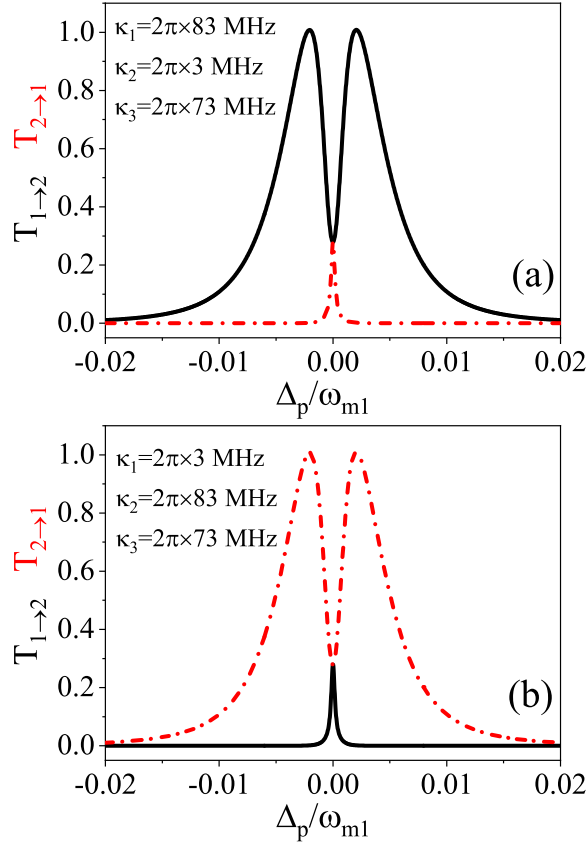


FIG. 4: Probe transmission intensities  $T_{2 \rightarrow 1}$  and  $T_{1 \rightarrow 2}$  as a function of probe-drive field detuning under different values of cavity decay rates: (a)  $\kappa_1/2\pi = 83$  MHz,  $\kappa_2/2\pi = 3$  MHz,  $\kappa_3/2\pi = 73$  MHz, and (b)  $\kappa_1/2\pi = 3$  MHz,  $\kappa_2/2\pi = 83$  MHz,  $\kappa_3/2\pi = 73$  MHz. The general parameters are given as,  $\Delta_1 = \Delta_2 = \Delta_3 = \omega_{m1}$ , whereas other parameter values are same as in Fig. 2.

The above discussion manifests non-reciprocity when the effective cavity detunings are slightly off-resonant with the mechanical excitations, whereas the back conversion (non-reciprocal to reciprocal) of transmission is also possible. Hence the effective cavity detuning can be used to flexibly control the bidirectional output-signal transfer at either port as demanded.

### B. Influence of optomechanical couplings on signal transmission

In cavity optomechanics, the optomechanical coupling strength between the intracavity photons and the NMR (which results from the radiation pressure of cavity photons on the NMR) plays a key role in inducing the non-linearity into the cavity optomechanical system. Here we study the influence of the optomechanical coupling strength in creating and controlling the bidirectional non-reciprocal response of the output probe fields across two available routes (ports). Unlike the Faraday's effect in

magneto-optical materials that makes the time-reversal symmetry breaking happen [9], the non-reciprocity in our proposed system arises due to the asymmetric radiation pressure of cavity photons on the NMRs when the optomechanical couplings are unequal. When there is a strong optomechanical interaction for cavity  $a_1$  (60 MHz) and relatively lower for cavity  $a_2$  (1.5 MHz), it exhibits a complete optical signal transfer at port 1 without any restriction at origin (shown by red dot-dashed peak), whereas in the same frequency range, the transmission of signal  $T_{1 \rightarrow 2}$  at port 2 is fully blocked as shown by the black solid curve depicted in Fig. 3(a). Due to destructive interference, i.e., in case of  $O_{m1} > O_{m2}$ , the signal is blocked in the  $T_{1 \rightarrow 2}$  direction, whilst at the same time, the signal transit becomes viable due to the reverse effect, that is, constructive interference at resonance conditions. The constructive/destructive interference effect between the mechanical excitations and probe-induced cavity field happens here due to the asymmetry of the radiation pressure on the NMRs [43], which comes into play because of the changes in cavity lengths since the optomechanical couplings depend on the cavity lengths, i.e.,  $O_{mi} = \frac{\omega_{ai}}{L_i} \sqrt{\frac{\hbar}{m_{eff,i}\omega_{mi}}}$  and  $O_{3i} = \frac{\omega_{a3}}{L_{3i}} \sqrt{\frac{\hbar}{m_{eff,i}\omega_{mi}}}$  ( $i = 1, 2$ ) [36], where  $L_i$  and  $L_{3i}$  are the cavity lengths and  $m_{eff,i}$  is the effective mass of NMR. The converse case happens when the optomechanical couplings satisfy  $O_{m2} > O_{m1}$  as given in Fig. 3(b). However, when the optomechanical couplings become equal/same, that is,  $O_{m1} = O_{m2}$ , the signal transmission behavior turns completely to reciprocal as a result of symmetric radiation pressure on both the NMRs. For example, when  $O_{m1} = O_{m2}$ , the signal is allowed to pass through both output ports by the same amount at the origin on the frequency axis (not shown here) which is reciprocal in nature. In our proposed setup, the optomechanical couplings, i.e.,  $O_{m31}$  and  $O_{m32}$  associated with cavity mode  $a_3$  and NMRs are of great interest in realizing non-reciprocal behavior of output fields. Non-reciprocity is valid as long as  $O_{m31}$  and  $O_{m32}$  are non-zero. In case, these couplings go down to zero, the non-reciprocity is lost and we are left with complete reciprocal signal transmission at output ports regardless of the values assigned to couplings  $O_{m1}$  and  $O_{m2}$  as shown in Fig. 3(c). Figure 3(c) shows maximum signal transfer for both ports at the origin when  $O_{m31} = O_{m32} = 0$  which has a reciprocal nature. Thus the above discussion justifies the fact that signal transmission at either port can be controlled flexibly from reciprocal to non-reciprocal and vice versa by modifying the optomechanical couplings.

### C. Effect of cavity decay rates on the signal flow

Every COS inherits intrinsic photons dissipation to external bath (cavity decay rate) that depends on the quality factor  $Q$  of the end mirrors. Similarly, in our proposed cavity setup, the cavity decay rate  $\kappa_i$  is inevitable

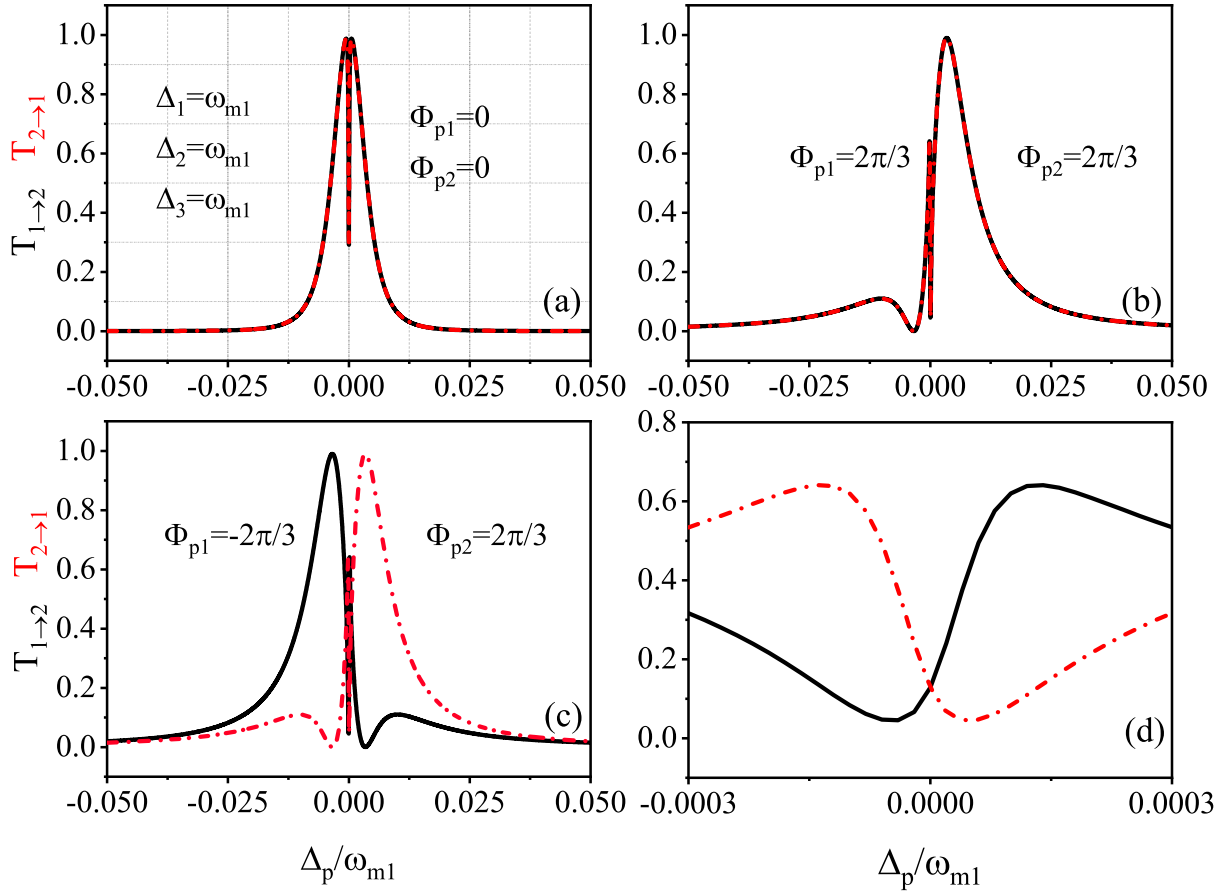


FIG. 5: Dependence of transmission intensities  $T_{2 \rightarrow 1}$  and  $T_{1 \rightarrow 2}$  on the probe-drive field detuning  $\Delta_p$  when (a) probe phases  $\Phi_{p1} = \Phi_{p2} = 0$ , (b)  $\Phi_{p1} = \Phi_{p2} = 2\pi/3$ , (c)  $\Phi_{p1} = -2\pi/3$ ,  $\Phi_{p2} = 2\pi/3$  and (d) The inset specifying transmission curves for  $T_{2 \rightarrow 1}$  and  $T_{1 \rightarrow 2}$  over a short range on frequency axis in (c). The general parameters are given as  $\Delta_1 = \Delta_2 = \Delta_3 = \omega_{m1}$ , and other parameter values are same as in Fig. 2.

and thus affects the bidirectional signal transfer. As the transmission happens via left and right ports, we consider changes in the cavity decay rates associated with cavities  $a_1$  and  $a_2$  only. In Fig. 4(a), when the cavity decay rates have  $\kappa_1 > \kappa_2$ , the system permits the output probe signal from port 1 to port 2 with maximum value (equal to 1) of  $T_{1 \rightarrow 2}$  as shown by two black colored peaks around origin, but blocks it in the opposite direction, i.e., from port 2 to port 1 with transmission value of  $T_{2 \rightarrow 1}$  equal to zero. The above relation between two decay rates insinuates the razing of photons in cavity  $a_1$  as compared to cavity  $a_2$  which eventually results in suppressing of optical signals through cavity  $a_1$  and thus to port 1. However, the signal is transferred efficiently in reverse direction  $T_{1 \rightarrow 2}$ . The larger amount of  $\kappa_1$  is responsible for lowering the photons number and thus the optomechanical coupling in cavity  $a_1$  as compared to  $\kappa_2$  value which results in comparatively larger optomechanical coupling in cavity  $a_2$  and thus time reversal symmetry breaking happens that accounts for the non-reciprocal transmission. At origin, both the transmission curves meet at a single point, the curve  $T_{1 \rightarrow 2}$

shows a dip, whereas  $T_{2 \rightarrow 1}$  has a short peak. Figure 4(b) reveals the case for signal transfer when  $\kappa_1 < \kappa_2$ , so the converse happens that provokes the signal transmission from port 2 to 1  $T_{2 \rightarrow 1}$  and suppresses it in the reverse direction, that is,  $T_{1 \rightarrow 2}$ . Hence, the cavity with larger value of  $\kappa$  blocks signal transfer at its respective port comming from the other one, while cavity with lower decay rate supports signal transmission at the same port. Thus, non-reciprocity can be observed by considering the cavity decay rates values where the signal transfer behavior can be manipulated.

#### D. Effect of probe and drive phases on signal flow

Generally, the phases of interacting fields play an important role in the interference phonomenon. Here we explain the significance of external probe and drive field phases that enables the cavity system to switch the signal transmission from reciprocal to non-reciprocal and vice versa. These phase changes from both inputs are analogous to the synthetic magnetic field that is respon-

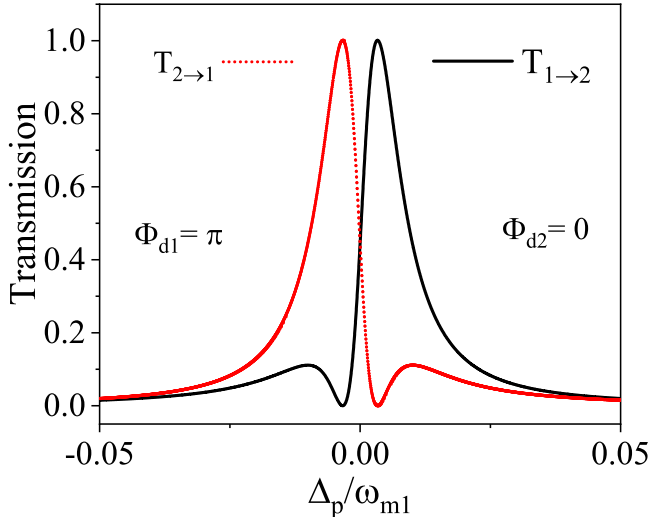


FIG. 6: Dependence of transmission intensities  $T_{2\rightarrow 1}$  and  $T_{1\rightarrow 2}$  on the probe-drive field detuning  $\Delta_p$  when probe phases  $\Phi_{p1} = -2\pi/3$ ,  $\Phi_{p2} = 2\pi/3$  and drive field phases  $\Phi_{d1} = \pi$ ,  $\Phi_{d2} = 0$ . The general parameter values are given as  $\Delta_1 = \Delta_2 = \Delta_3 = \omega_{m1}$ . All other values are same as in Fig. 2.

sible for breaking time reversal symmetry and can be used as bidirectional non-reciprocal signal transport device [44]. First, we suppose that the incoming external probe fields from either ports have no phase change, that is,  $\Phi_{p1} = \Phi_{p2} = 0$ . We report a complete reciprocal signal transfer via both ports with two transmission peaks ( $T_{1\rightarrow 2} = T_{2\rightarrow 1} = 1$ ) symmetric around the origin separated by a short dip at origin as shown in Fig. 5(a). Now, when the phases of the probe fields are changed to  $\Phi_{p1} = \Phi_{p2} = 2\pi/3$ , we still obtain a reciprocal transmission curve with Fano-like profile shown by Fig. 5(b). As we change the sign of any of the probe phases, i.e.,  $\Phi_{p1} = -2\pi/3$  and  $\Phi_{p2} = 2\pi/3$ , the transmission is shifted from reciprocal to non-reciprocal shown by Fano-like curves in Fig. 5(c). The direction of non-reciprocal transmission completely reverses when the phases signs are changed, that is,  $\Phi_{p1} = 2\pi/3$  and  $\Phi_{p2} = -2\pi/3$ . The same result given in Fig. 5(c) can be achieved for the phase changes equal to  $\Phi_{p1} = \pi/3$  or  $\Phi_{p2} = -\pi/3$ . Figure 5(d) shows the inset of Fig. 5(c) curve over a short frequency range where sharp exchange of non-reciprocal signal transmission happens and follow an envelop like shape. The curves shown in inset also show non-reciprocity since at the same time increasing behavior of one curve is seen along with decreasing tendency of other curve.

Now, following the explanation in the above context, we check the sensitivity of the system to the external drive-field phase regarding the non-reciprocal signal

transfer. In Fig. 6, the COS setup delivers absolute non-reciprocal transmission across both ports when either of the drive field phase is tuned to  $\pi$  radian, that is,  $\Phi_{d1} = \pi$ ,  $\Phi_{d2} = 0$  or vice versa. Compared to Fig. 5(c) where two extra/additional transmission peaks exist close to origin, we observe those two extra peaks being vanished when the drive field phase is changed to  $\Phi_{d1} = \pi$  and we report only single transmission peak having Fano-like asymmetric profile for  $T_{1\rightarrow 2}$  and a complete blockade for  $T_{2\rightarrow 1}$  at the same time on the positive frequency axis. Similarly, on the left of origin, a transmission peak for  $T_{2\rightarrow 1}$  and signal blockade for  $T_{1\rightarrow 2}$  can be observed at the same frequency. When both drive-field phases are set to  $\Phi_{d1} = \Phi_{d2} = \pi$ , the transmission curve shown in Fig. 5(c) can be regained.

From the above description, it is clear that our proposed COS setup is phase-sensitive and non-reciprocal signal transfer is possible by changing the phases of the external probe fields and drive fields.

#### IV. SUMMARY

We have investigated the non-reciprocal behavior of output probe field through a bidirectional multi-mode COS with a beam splitter. A perfect non-reciprocal transmission of signal due to the breaking of time reversal symmetry is revealed at the effective cavity detunings  $\Delta_1$ ,  $\Delta_2$  close to mechanical frequency, and a full duplex transmission is noted by adjusting the  $\Delta_1$ ,  $\Delta_2$  values. By modifying the optomechanical couplings, signal transfer has been blocked from passing via one port (terminal) and passed on through other at resonance conditions. A non-reciprocal signal transfer is affected by tuning the cavity decay rates, which are the intrinsic parameters that can not be omitted. Furthermore, the phase changes associated with input probe and drive fields from either port have crucial impact on the signal transport and the transmission from reciprocal to non-reciprocal and vice versa. Our proposed theoretical model could be the right route for experimentalists to explore a new and efficient way for manufacturing non-reciprocal devices like routers, optical isolators, sensors, light diodes, and full duplex signal transmitters and transducers.

#### Acknowledgments

This research is supported by the National Natural Science Foundation of China (grant Nos. 11974309 and 11674284), Zhejiang Provincial Natural Science Foundation of China under Grant No. LD18A040001, and the grant by National Key Research and Development Program of China (No. 2017YFA0304202).

[1] D. L. Sounas and A. Alù, Nat. Photonics **11**, 774 (2017).

[2] H. A. Lorentz, Amsterdamer Akademie

der Wetenschappen **4**, 176 (1896); <https://ci.nii.ac.jp/naid/10018471922/en/>

[3] M. Levy, J. Opt. Soc. Am. B **22**, 254 (2005).

[4] T. R. Zaman, X. Guo, and R. J. Ram, Appl. Phys. Lett. **90**, 023514 (2007).

[5] H. Dotsch, N. Bahlmann, O. Zhiromskyy, M. Hammer, L. Wilkens, R. Gerhardt, P. Hertel, and A. F. Popkov, J. Opt. Soc. Am. B **22**, 240 (2005).

[6] Z. Wang, Y. Chong, J. D. Joannopoulos, and M. Soljačić, Nature (London) **461**, 772 (2009).

[7] A. B. Khanikaev, S. H. Mousavi, G. Shvets, and Y. S. Kivshar, Phys. Rev. Lett. **105**, 126804 (2010).

[8] L. Bi, J. Hu, P. Jiang, D. H. Kim, G. F. Dionne, L. C. Kimerling, and C. A. Ross, Nat. Photonics **5**, 758 (2011).

[9] J. Y. Chin, et al., Nat. Commun. **4**, 1599 (2013).

[10] D. Dai, J. Bauters, and J. E. Bowers, Light Sci. Appl. **1**, e1 (2012).

[11] N. A. Estep, D. L. Sounas, J. Soric, and A. Alù, Nat. Phys. **10**, 923 (2014).

[12] J. Kerckhoff, K. Lalumière, B. J. Chapman, A. Blais, and K. W. Lehnert, Phys. Rev. Appl. **4**, 034002 (2015).

[13] L. Ranzani and J. Aumentado, New J. Phys. **16**, 103027 (2014).

[14] T. C. White et al., Appl. Phys. Lett. **106**, 242601 (2015).

[15] C. Macklin et al., Science **350**, 307 (2015).

[16] S. Hua, J. Wen, X. Jiang, et al., Nat. Commun. **7**, 13657 (2016).

[17] M. Hafezi and P. Rabl, Opt. Express, **20**, 7672 (2012).

[18] Z. Shen et al., Nat. Photonics, **10**, 657 (2016).

[19] Z. Shen et al., Nat. Commun. **9**, 1797 (2018).

[20] S. J. M. Habraken, K. Stannigel, M. D. Lukin, and P. Zoller, New J. Phys. **14**, 115004 (2012).

[21] X.-W. Xu, and Y. Li, Phys. Rev. A **91**, 053854 (2015).

[22] B.-Y. Zhou and G.-x., Li, Phys. Rev. A **94**, 033809 (2016).

[23] H. Tan, W. Deng, Q. Wu, G. Li, Phys. Rev. A **95**, 053842 (2017).

[24] M. U. Rahman, I. Ahmad, S. Qamar, and others, Euro phys. Lett. **120**, 24001 (2018)

[25] M. Ullah, A. Abbas, J. Jing, L.-G. Wang, Phys. Rev. A **100**, 063833 (2019).

[26] K. Qu and G. S. Agarwal, Phys. Rev. A **87**, 063813 (2013).

[27] T. Kipf and G. S. Agarwal, Phys. Rev. A **90**, 053808 (2014).

[28] L.-G. Si, H. Xiong, M. S. Zubairy, and Y. Wu, Phys. Rev A **95**, 033803 (2017).

[29] G. A. Peterson et al., Phys. Rev. X **7**, 031001 (2017).

[30] N. R. Bernier, L. D. Tóth, A. Koottandavida, M. A. Ioannou, D. Malz, A. Nunnenkamp, A. K. Feofanov, and T. J. Kippenberg, Nat. Commun. **8**, 604 (2017).

[31] S. Barzanjeh et al., Nat. Commun. **8**, 953 (2017).

[32] X.-W. Xu, Y. Li, A.-X. Chen, and Y.-X. Liu, Phys. Rev. A **93**, 023827 (2016).

[33] L. Tian and Z. Li, Phys. Rev. A **96**, 013808 (2017).

[34] L. Mercier de Lépinay, C. F. Ockeloen-Korppi, D. Malz, and M. A. Sillanpää, Phys. Rev. Lett. **125**, 023603 (2020).

[35] G. S. Agarwal and S. Huang, Phys. Rev. A **81**, 041803(R) (2010).

[36] M. J. Akram, M. M. Khan, and F. Saif, Phys. Rev. A **92**, 023846 (2015).

[37] Q. He et al., Ann. Phys. (Berlin) **2000612** (2021).

[38] G. S. Agarwal and S. Huang, New J. Phys. **16**, 033023 (2014).

[39] D. F. Walls and G. J. Milburn, Quantum Optics, Berlin: Springer-Verlag, Berlin, (1994).

[40] X. B. Yan, C. L. Cui, K. H. Gu, X. D. Tian, C. B. Fu, and J. H. Wu, Opt. Express **22**(5), 4886 (2014).

[41] X.-W. Xu, L. N. Song, Q. Zheng, Z. H. Wang, and Y. Li Phys. Rev. A **98**, 063845 (2018).

[42] Kharel et al., Sci. Adv. **5**, eaav0582 (2019).

[43] S. Manipatruni, J. T. Robinson, and M. Lipson, Phys. Rev. Lett. **102**, 213903 (2009).

[44] F. Ruesink, J. P. Mathew, M. A. Miri, A. Alù, and E. Verhagen, Nat. Commun. **9**, 1798 (2018).